MOLECULAR PHYSICS, 1988, VOL. 65, NO. 6, 1505–1524

The P_4 model and its orientational phase transition

by C. CHICCOLI and P. PASINI
INFN Sez. di Bologna and CNAF, Via Mazzini, 2, 40138 Bologna, Italy

F. BISCARINI and C. ZANNONI
Dipartimento di Chimica Fisica ed Inorganica, Università,
Viale Risorgimento, 4, 40136 Bologna, Italy

(*Received 25 April 1988; accepted 25 July 1988*)

A simple generalization of the Lebwohl–Lasher model, where fourth rank, rather than second rank, interactions are involved is investigated. This model was first put forward and studied some years ago using molecular field theory (Zannoni, C., 1979, *Molec. Crystals liq. Crystals Lett.*, **49**, 247). There it was found that there should be a temperature interval where the fourth rank order parameter is higher than the second rank one. This unusual behaviour has been found by various groups to be consistent with fluorescence depolarization data for diphenylhexatriene in DPPC and DMPC membrane vesicles. In this paper we investigate more thoroughly the P_4 model using Monte Carlo simulations with periodic boundary conditions on a $10 \times 10 \times 10$ lattice and with the recently proposed Cluster Monte Carlo method on a $6 \times 6 \times 6$ and a $10 \times 10 \times 10$ lattice. Our results are consistent with a first order transition. We find that the results for the transition temperature and for the second and fourth rank order parameters are well approximated by two site cluster theory.

1. The P_4 model

We generally define a P_4 model as a system of particles interacting with a purely fourth rank pair potential [1]. Here we are more specifically concerned with a lattice version of the model defined by the rotationally invariant hamiltonian

$$U_N(\omega_1, \omega_2, \ldots, \omega_N) = -\frac{1}{2}\sum_{i=1}^{N}\sum_{j=1}^{N}\varepsilon_{ij}P_4(\cos\beta_{ij}); \qquad \text{with } i \neq j, \tag{1}$$

where it is understood that the particles are placed on a regular three dimensional cubic lattice with an edge of length L, containing therefore a total of $N = L^3$ sites, β_{ij} measures the angle between the symmetry axes of the two molecules, $P_4(x)$ is a fourth rank Legendre polynomial and ε_{ij} designates the strength of nearest neighbour attractive interactions. Thus ε_{ij} is either zero or a positive constant, ε. The lattice model is a generalization to fourth rank of the well known Lebwohl–Lasher model [2]. The simple interaction (1) has two minima for molecules parallel or perpendicular to each other, as shown in figure 1. The configuration of the system is given by the set of N orientations $\omega_i = (\alpha_i, \beta_i)$ [3]. A P_4 model was first put forward and studied some years ago using molecular field theory [1]. There it was found that the first-order character of the disordering transition is enhanced compared to the second rank case. Moreover it was found that there should be a temperature interval where the fourth rank order parameter is higher than the second rank one.

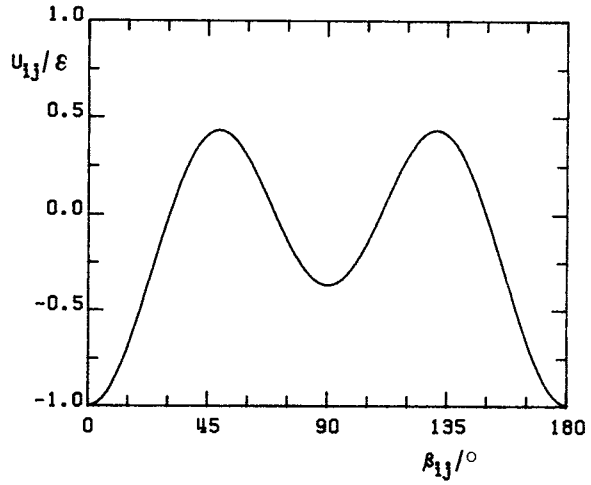

Figure 1. The anisotropic pair potential U_{ij} (dimensionless units) for two neighbour molecules in the P_4 model as a function of the relative angle β_{ij} (degrees).

Quite recently this unusual behaviour has been found to be consistent with fluorescence depolarization data of diphenylhexatriene in DPPC and DMPC membrane vesicles [4–6]. The reason could lie in the fact that the orientational distribution predicted for the model has a peak not only parallel to the director but also perpendicular to it, even though this is a smaller one. The model could thus roughly emulate physical situations with two perpendicular sites populated. Here we have investigated the P_4 model with computer simulations [7] using the recently proposed Cluster Monte Carlo (CMC) method [8] on a $6 \times 6 \times 6$ and a $10 \times 10 \times 10$ lattice and the Periodic Boundary Monte Carlo (PBMC) on a $10 \times 10 \times 10$ lattice. We also show that two site cluster (TSC) theory [9–12] gives a good approximation to the computer experimental results.

2. Monte Carlo simulations

2.1. *Cluster Monte Carlo*

An important aspect of the computer simulation of anisotropic systems is the determination of their temperature of transition to the isotropic phase. To this end the choice of boundary conditions, i.e. the environment which surrounds the sample, is important. Two common choices are to use periodic boundary conditions or to leave empty space around the box. The first method is the standard one in simulations and consists of having exact replicas of the system filling the space as required by the range of the pair interaction. Although vastly superior to a free space boundary, periodic boundary conditions can lead to a smearing and broadening of the variation of the heat capacity and order parameter with temperature. This complicates the location of the transition and in turn often means that relatively large samples, with many thousands of particles may have to be used. In this paper we have first simulated the P_4 system using the recently proposed Cluster Monte Carlo method. In this technique, described in detail in [8], the desired bulk or global average of a quantity A is written as an average over all the external 'world' configurations [W] of the values $\langle A \rangle_{[W]}$ calculated for a fixed configuration of the

'world' outside the sample box. Thus

$$\langle A\rangle_G = \langle\langle A\rangle_{[W]}\rangle_W \tag{2a}$$

$$\approx (1/M_W)\sum_{[W]}\langle A\rangle_{[W]} \tag{2b}$$

where M_W is the number of sampling used in the approximation (2*b*). In practice a MC simulation is run to obtain $\langle A\rangle_{[W]}$ and the outside world configurations needed are obtained by creating a zone of ghost particles outside the sample box having on average the same ordering properties and, in particular, the same singlet distribution of the system inside the box. The orientations of the virtual neighbours are sampled from an orientational distribution function constructed, using maximum entropy principles, from the order parameters calculated inside the sample. We assume a symmetry breaking field direction, defining the Z laboratory axis and that the ordered phase is at most uniaxial around this direction. We then calculate the order parameters with respect to this direction, which for cylindrically symmetric particles are just the Legendre polynomial averages $\langle P_L\rangle$, with L even, i.e. $\langle P_2\rangle$, $\langle P_4\rangle$, ..., $\langle P_{L'}\rangle$. We construct the best information theory [13] inference for the orientational distribution of the particles outside the sample based on these observables, i.e.

$$P(\cos\beta) = \exp\left[\sum_{L=0}^{L'} a_L P_L(\cos\beta)\right], \tag{3}$$

where the coefficients a_L are determined from the constraint that the available $\langle P_L\rangle$ can be reobtained by averaging $P_L(x)$ over the distribution. In the present case we calculate the first two relevant order parameters, $\langle P_2\rangle$ and $\langle P_4\rangle$, so that the most likely distribution will be of the form

$$P(\cos\beta) = \frac{\exp\left[a_2 P_2(\cos\beta) + a_4 P_4(\cos\beta)\right]}{\int_0^\pi d\beta \sin\beta \exp\left[a_2 P_2(\cos\beta) + a_4 P_4(\cos\beta)\right]}. \tag{4}$$

The coefficients a_2, a_4 are determined by solving the non linear system

$$\langle P_2\rangle = \frac{\int_0^\pi d\beta \sin\beta P_2(\cos\beta)\exp\left[a_2 P_2(\cos\beta) + a_4 P_4(\cos\beta)\right]}{\int_0^\pi d\beta \sin\beta \exp\left[a_2 P_2(\cos\beta) + a_4 P_4(\cos\beta)\right]}, \tag{5a}$$

$$\langle P_4\rangle = \frac{\int_0^\pi d\beta \sin\beta P_4(\cos\beta)\exp\left[a_2 P_2(\cos\beta) + a_4 P_4(\cos\beta)\right]}{\int_0^\pi d\beta \sin\beta \exp\left[a_2 P_2(\cos\beta) + a_4 P_4(\cos\beta)\right]}. \tag{5b}$$

The solution of this system is obtained using the IMSL library routines [14]. The results are shown in figure 2. Notice that the coefficients $a_2(\langle P_2\rangle, \langle P_4\rangle)$ and $a_4(\langle P_2, \langle P_4\rangle)$ are not defined in the entire $(\langle P_2\rangle, \langle P_4\rangle)$ plane, but in a sort of half-moon region. This domain is delimited by the inequalities [15]

$$\tfrac{35}{18}\langle P_2\rangle^2 - \tfrac{5}{9}\langle P_2\rangle - \tfrac{7}{18} \leqslant \langle P_4\rangle \leqslant \tfrac{5}{12}\langle P_2\rangle + \tfrac{7}{12}, \tag{6}$$

and these restrictions follow in turn from Schwarz's inequality [16] applied to the specific trigonometric form of the second and fourth rank Legendre polynomials.

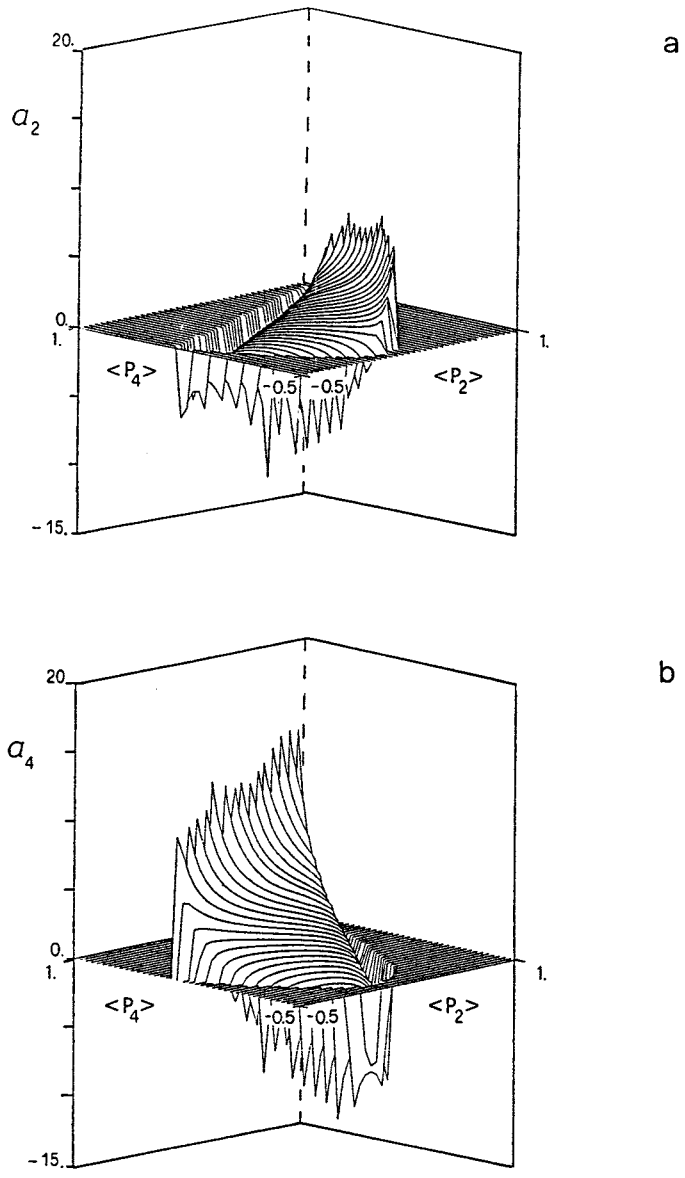

Figure 2. The exponential coefficients a_2 (*a*) and a_4 (*b*) in the distribution $f(\beta) \propto \exp [a_2 P_2(\cos \beta) + a_4 P_4(\cos \beta)]$ shown as a function of $\langle P_2 \rangle$ and $\langle P_4 \rangle$.

We have studied two systems of particles interacting with the P_4 potential equation (1) on a simple cubic lattice with dimensions $6 \times 6 \times 6$ and $10 \times 10 \times 10$. The calculation is started from a completely aligned system at low temperatures or, where available, from an already equilibrated configuration at the lower temperature. The Metropolis Monte Carlo procedure is then used to update the lattice for a certain number of cycles, i.e. of sets of N attempted moves. Each particle is selected at random for trial move at every cycle using a random shuffling algorithm [17]. A new trial orientation of the chosen particle is then generated by a controlled

variation from the previous one using the Barker–Watts technique [18]. We have checked that a rejection ratio not too far from 0·5 is achieved. For the present system we have found the simpler method of generating uniformly distributed random values of cos β and α unsatisfactory, since it leads to a very small acceptance ratio. After a pre-equilibration period the order parameters $\langle P_2 \rangle$, $\langle P_4 \rangle$ inside the sample are calculated. These two parameters are used to determine a_2 and a_4 and thus the distribution in (4) from which new orientations for the ghost particles outside the box are sampled. We generate the orientations of these external ghost molecules using a simple rejection technique [8] and check that both the order parameters $\langle P_2 \rangle_{\text{out}}$ and $\langle P_4 \rangle_{\text{out}}$ relative to the particles outside are the same as those inside within an acceptable error (here 0·006) and the generation is repeated if this is not the case. The energy of the system is then recalculated and evolution proceeds as before. In all the subsequent cycles the order parameters with respect to the Z laboratory direction P_L^J for the molecules inside the box are still calculated. After a certain number of cycles M an average is calculated for this K trajectory segment together with the attendant standard deviation σ_K. These $\langle P_2 \rangle_{\text{in}}$ and $\langle P_4 \rangle_{\text{in}}$ parameters are then compared to the ones outside and if the difference between them is statistically significant to within a particular confidence level (here 0·05) [19], a new set of orientations for the ghost molecules is generated using the new order parameters. If the order parameters inside and outside are not significantly different the orientations outside are kept and the next check is made after a longer segment, i.e. $M_{K+1} > M_K$. The number of cycles M_K is instead left unchanged if the order is adjusted. This ensures that on one hand we do not choose incorrect order parameters outside and leave them unchanged. On the other hand since every change of the outside layer will lower the short range correlation at the interface this method takes care to do the updating only if really needed and not on every cycle or on the basis of some wild fluctuation. A number of observables are calculated, as we shall see in detail later on.

2.2. *Periodic boundary conditions*

Since the CMC method is relatively new and has only been applied to the Lebwohl–Lasher model [8] it is of interest to compare its performance with the classical PBMC method. Thus we have also studied a system of $N = 1000$ particles employing the standard Monte Carlo Metropolis method with periodic boundary conditions (see, e.g. [7]). The simulation was meant to be completely independent from the previous CMC ones, so once more the run at the lowest temperature studied has been initiated from a completely aligned system. The calculations at the other temperatures have been started from an equilibrium configuration at the nearest lower temperature. A separate simulation starting from the isotropic phase has also been performed to check for hysteresis effects. The same controlled configuration updating procedure mentioned in the previous section [18] was employed. Order parameters have been evaluated by diagonalization of the ordering matrix [7] and fourth rank order parameters have been computed with the algorithm introduced in [17].

3. Two site cluster theory

Here we only give a short summary of the two site cluster theory employed, since our treatment follows closely the lines of the classic work of Strieb, Callen and

Horwitz [9] and to some extent those of the more recent applications of Lekkerkerker *et al.* [12, 20] on the Lebwohl–Lasher model (see, e.g. [7]). The key point of the cluster treatment is to devise an approximation for the Helmholtz free energy A_N as a sum of contributions from progressively larger clusters. Here

$$A_N = -kT \ln Z_N \tag{7}$$

and Z_N is the N particle configurational partition function

$$Z_N = \frac{1}{N!} \int \{d\omega\} \exp [-U_N(\omega_1, \omega_2, \ldots, \omega_N)/kT], \tag{8}$$

where the molecular orientations are referred to the laboratory frame, chosen with the z axis along the potential director. The volume element is $\{d\omega\} = d\omega_1 d\omega_2 \ldots d\omega_N$, with $d\omega_i = d\alpha_i \sin \beta_i d\beta_i$, and the integration is extended to all the variables not appearing on the left hand side. We proceed by rewriting the relative orientation terms $P_4(\cos \beta_{ij})$ in the potential energy (1) as a sum of Wigner functions using the spherical harmonics addition theorem [3] as

$$U_N = -\varepsilon \sum_{i<j} \{P_4(\cos \beta_i) P_4(\cos \beta_j) + \sum_{q \neq 0} D^4_{q0}(\omega_i) D^{4*}_{q0}(\omega_j)\}. \tag{9}$$

The potential energy can be formally partitioned into an unperturbed part U^0 containing only single particle contributions and a perturbation term U'

$$U_N = U^0 + U', \tag{10}$$

where

$$U^0 = -\varepsilon \sum_{i<j} \{-b_4^2 + b_4[P_4(\cos \beta_i) + P_4(\cos \beta_j)]\} \tag{11}$$

and

$$U' = -\varepsilon \sum_{i<j} \{P_4(\cos \beta_{ij}) + b_4^2 - b_4[P_4(\cos \beta_i) + P_4(\cos \beta_j)]\}. \tag{12}$$

The arbitrary separation constant b_4 is to be treated as an adjustable variational parameter and will be determined by requiring that the free energy is a minimum. As a consequence of the separation introduced in the potential, the free energy becomes a sum of two parts

$$A_N = A^0 + A' \tag{13}$$

where the unperturbed part

$$\begin{aligned} -A^0/(kT) &= \ln \int \{d\omega\} \exp (-U^0/kT), \\ &= -\frac{Nz\varepsilon}{2kT} b_4^2 + N \ln Z_1 - N \ln 2 \end{aligned} \tag{14}$$

consists only of one particle contributions, with z the coordination number ($z = 6$ in our case) and Z_1 is a single particle pseudo-partition function

$$Z_1 = \int_0^\pi d\beta \sin \beta \exp \left\{\frac{z\varepsilon}{kT} b_4 P_4(\cos \beta)\right\}. \tag{15}$$

At this level of approximation, the treatment would be equivalent, after minimization with respect to b_4, to molecular field theory and it would yield $b_4 = \langle P_4 \rangle$. An improvement over molecular field is obtained by approximating the correction term $-A'$,

$$-A'/(kT) = \ln \langle \exp(-U'/kT) \rangle_{U^0} \tag{16}$$

in (13). Following Strieb–Callen–Horwitz [9] the correction free energy can be formally expanded in an infinite cluster series as

$$-A'/(kT) = -\sum_{\alpha=2} A'_\alpha/(kT), \tag{17}$$

where the explicit general expression for the α cluster contribution is given in [9]. In practice we retain here the first correction term, obtaining the so called two site cluster approximation

$$-A'/(kT) \approx -A'_2/(kT) \tag{18a}$$

$$= \sum_{i<j} \ln \langle \exp[-U'_{ij}/(kT)] \rangle_{U^0} \tag{18b}$$

$$= \tfrac{1}{2} Nz \ln Z_{12} - \frac{Nz\varepsilon}{2kT} b_4^2 - Nz \ln Z_1. \tag{18c}$$

The approximate free energy at two-site cluster level then becomes

$$-A_2/(kT) = -(A^0 + A'_2)/kT \tag{19a}$$

$$= \tfrac{1}{2} Nz \ln Z_{12} - (z-1)N \ln Z_1, \tag{19b}$$

where Z_{12} is the two particle pseudo-partition function

$$Z_{12} = \int d\omega_1 \int d\omega_2 \exp\left\{\frac{\varepsilon}{kT}[b_4(z-1)[P_4(\cos\beta_1) + P_4(\cos\beta_2)] + P_4(\cos\beta_{12})]\right\}. \tag{20}$$

The condition of minimum free energy with respect to b_4 gives the consistency requirement

$$\langle P_4 \rangle_{Z_1} = \tfrac{1}{2} \langle P_4(\cos\beta_1) + P_4(\cos\beta_2) \rangle_{Z_{12}}. \tag{21}$$

In practice we shall refer the free energy to the standard isotropic state with complete disorder, thus we shall subtract the infinite temperature contribution. The various thermodynamic observables are obtained from the free energy. The energy is obtained by differentiating the free energy with respect to $\beta_T \equiv 1/(kT)$ and inserting the self-consistency conditions. This gives

$$\langle U_N \rangle = -\frac{Nz\varepsilon}{2} \sigma_4, \tag{22}$$

where σ_4 is a short range order parameters

$$\sigma_L = \langle P_L(\cos\beta_{12}) \rangle_{Z_{12}}. \tag{23}$$

equal to the value of the rotationally invariant pair correlation at nearest neighbours distance $r = a$ [7]

$$\sigma_L = G_L(a). \tag{24}$$

The ability to calculate short range order parameters represents an important advantage of two site cluster theory over mean field. There in fact the relative order of two particles is the same for arbitrary separations and $\sigma_L = \langle P_L \rangle^2$. In particular no short range order is predicted in the isotropic phase. An expression for the TSC heat capacity is obtained differentiating the energy with respect to temperature. Thus $C_V^* \equiv C_V/kN$ is

$$C_V^* = \frac{z\varepsilon^2}{2(kT)^2}\left\{[\langle P_4(\cos\beta_{12})^2\rangle - (\sigma_4)^2] + 2(z-1)\frac{\partial(\beta_T b_4)}{\partial\beta_T}\right.$$
$$\left.\times\,[\langle P_4(\cos\beta_1)P_4(\cos\beta_{12})\rangle_{Z_{12}} - \sigma_4\langle P_4(\cos\beta_1)\rangle_{Z_1}]\right\}, \qquad (25)$$

where $\partial(\beta_T b_4)/\partial\beta_T$ is obtained by differentiating both sides of the consistency equations with respect to the variational parameters at convergence. This gives

$$\frac{\partial(\beta_T b_4)}{\partial\beta_T} = \{\langle P_4(\cos\beta_1)P_4(\cos\beta_{12})\rangle_{Z_{12}} - \langle P_4(\cos\beta_1)\rangle_{Z_1}\sigma_4\}$$
$$\times\,\{z\langle P_4(\cos\beta_1)^2\rangle_{Z_1} - (z-1)[\langle P_4(\cos\beta_1)^2\rangle_{Z_{12}}$$
$$+\,\langle P_4(\cos\beta_1)P_4(\cos\beta_2)\rangle_{Z_{12}}]$$
$$+\,(z-2)\langle P_4(\cos\beta_1)\rangle_{Z_1}^2\}^{-1}. \qquad (26)$$

The numerical part of the problem is tackled by direct minimization of the free energy (equation (19)) in terms of the variational parameter. The MINUIT package from the CERN library [21] is used for this purpose. Calculation of the pseudo-partition Z_{12}, equation (20), can be reduced, after a simple change of variables, to a three dimensional integration. The minimization process is relatively time consuming, since these integrations have to be repeatedly performed at every step of the minimization process. The calculation is performed using a 32 point gaussian quadrature formula in each dimension and simplified exploiting as far as possible the symmetry of the integrand. Consistency checks have been run to ensure that the solution obtained is a true minimum and that sufficient numerical accuracy has been achieved.

4. Results and discussion

Here we present the results of the $10 \times 10 \times 10$ and $6 \times 6 \times 6$ CMC and of the $10 \times 10 \times 10$ PBMC simulations and compare them with the two site cluster findings. As we shall see in detail, the system undergoes an orientational phase transition at a reduced temperature $T^* = kT/\varepsilon$ around 0·650. In this transition region the simulations presented some difficulties of convergence and very long runs were required. For the PBMC simulation we have used at least 8000 equilibration cycles far from the transition and 18 000 in the pseudo-critical region. For the two CMC simulations we have discarded at least 11 000 and 20 000 equilibration cycles before starting production respectively when far or near the transition. In figure 3 we show the evolution of the energy per particle $U^* = U/N\varepsilon$ as a function of the number of cycles at a temperature below, near and above the transition. We indicate with an arrow the beginning of the production sequence. The significant increase of fluctuations at the middle temperature is readily apparent.

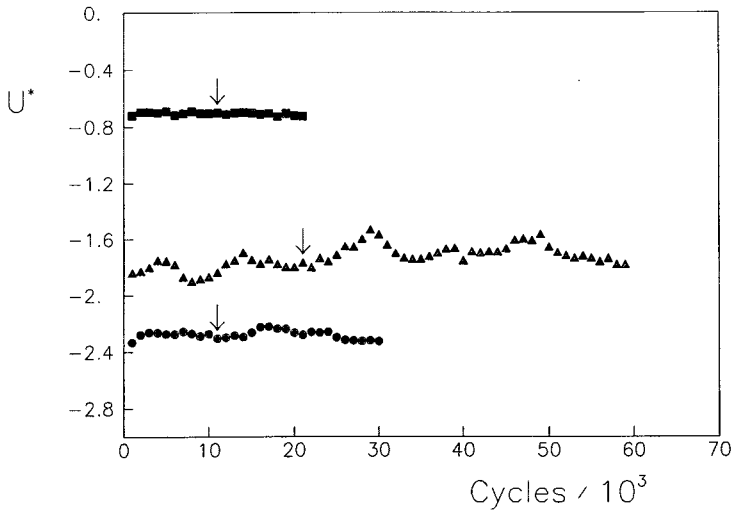

Figure 3. Evolution of the energy U^* with Monte Carlo cycles for a temperature below, near and above the transition, i.e. $T^* = 0{\cdot}580$ (black dots), $T^* = 0{\cdot}640$ (triangles) and $T^* = 0{\cdot}660$ (squares), as obtained by the CMC method on a $10 \times 10 \times 10$ lattice. The start of the production run is indicated by the arrow.

Apart from equilibration, production runs were also of varying length, according to the distance from the transition. Close to the phase change sequences as long as 100 kcycles have been used for the $6 \times 6 \times 6$ lattice and for the PBMC simulation. Runs were up to 70 kcycles for the $10 \times 10 \times 10$ CMC simulation. Each calculation was divided in chains of 1000 to 2000 cycles. Statistical errors were estimated as standard deviations from the average over these runs. During the production run various observables have been calculated in addition to the internal energy and second rank order parameters calculated at every cycle as already described. Every property of interest, A, is evaluated at every cycle. After a certain number of cycles m_J (typically between 1000 and 2000) an average A^J is calculated thus providing an effective coarse graining of the trajectory. A further grand average is then computed as the weighted average over M such supposedly uncorrelated segments. The attendant weighted standard deviation from the average σ_A is also calculated and gives the error estimates shown in the figures. We have calculated for each simulation energy, second and fourth rank order parameters. Pair correlation coefficients again of second and fourth rank have been calculated at selected temperatures.

4.1. *Heat capacity and phase transition*

The heat capacity of the system has been evaluated from the internal energy $\langle U_N \rangle$. Although conceptually this just requires a numerical differentiation, the straightforward procedure turns out to be quite complicated in practice, since we have data affected by some numerical simulation error as well as a very rapid change of the energy in a small temperature interval, corresponding to the disordering phenomena. Thus, on one hand, we would need to smooth the data to minimize the spurious effects of 'experimental' noise, while on the other we would call for precautions to avoid a smearing out of the C_V^* peak. Here, as in previous work [22], we take the view of treating the whole temperature interval at once and

we obtain the heat capacity by solving the integral equation (in reduced units)

$$U^*(T^*) = U(T_0^*) + \int_{T_0^*}^{T^*} dT^{*\prime}\, C_V^*(T^{*\prime}). \tag{27}$$

with an inversion method. The energies determined at a set of temperatures, $U^*(T_i^*)$ are used to build a M components vector of reduced energy differences $\mathbf{u}$. We can thus write

$$u_i = \int_{(i)} dT^{*\prime}\, C_V^*(T^{*\prime}) \tag{28}$$

where the integral is extended to the ith energy interval. Choosing to calculate C_V^* at a grid of K temperatures and employing a suitable numerical integration formula we reduce the integral equation to the matrix equation

$$\mathbf{C} = \mathbf{W}^{\mathrm{I}}\mathbf{u} \tag{29}$$

where $\mathbf{W}^{\mathrm{I}}$ is the generalized inverse [23] of the weights matrix $\mathbf{W}$ for the chosen numerical integration procedure. Here we have taken Simpson's integration formula and calculated $\mathbf{W}^{\mathrm{I}}$ according to Rust *et al.* [23]. The heat capacity has also been calculated independently by interpolating and smoothing the energy data using a five point orthogonal formula before performing a standard numerical differentiation. For the present system the results are similar to the previous ones. The estimate of errors in heat capacity calculations is rather complicated because of the numerical schemes employed. We have thus adopted the following simulation procedure. First we generate a rather large (here 100) number of plausible energy vs. temperature curves by sampling energy values at each temperature from a gaussian distribution of width given by the known standard deviation from the mean at that point. We then repeat the heat capacity calculation for every curve and obtain a set of C_V^* values whose average and standard deviation are our final reported results. The heat capacity and standard deviation errors obtained in this way are given in figure 4 for the various systems studied. We also show as the continuous line the two site cluster theory predictions.

The temperature of transition from nematic to isotropic is located by determining the maximum in the heat capacity as a function of temperature. We notice that the specific heat anomaly is very sharp for the P_4 potential and is in a broad sense fairly similar for all the methods employed. However, the Cluster Monte Carlo method gives the most pronounced peak in C_V^* and thus the easiest location of the transition. The small $6 \times 6 \times 6$ system treated with cluster boundary conditions gives results comparable to the PBMC $10 \times 10 \times 10$. The transition temperatures and the heat capacity are reported in the table.

The simulation on the small system of 216 particles, which is quite fast, allows an accurate location of the transition, as seen from the table. We see that the two site cluster theory overestimates the transition, but that, in contrast to the molecular field theory, it yields a value comparable to the simulations. Thus it predicts a first order phase transition at $T^* = 0{\cdot}663$ (3 per cent increase over the CMC result), as compared to a value of 0·751 (16 per cent increase) obtained from mean field theory. The character of the transition signalled by the MC simulation is consistent with first order behaviour. We notice that the aim of the present paper is not to establish this first order character beyond doubt. Indeed a finite size scaling study would be

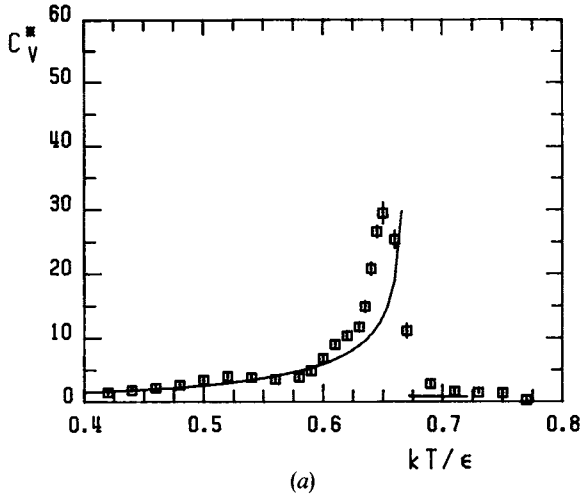

(*a*)

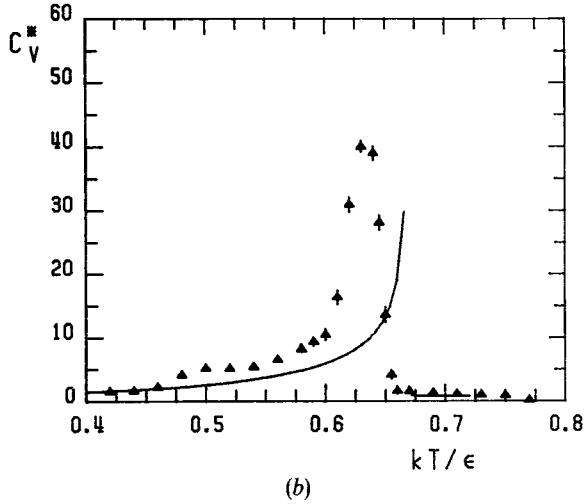

(*b*)

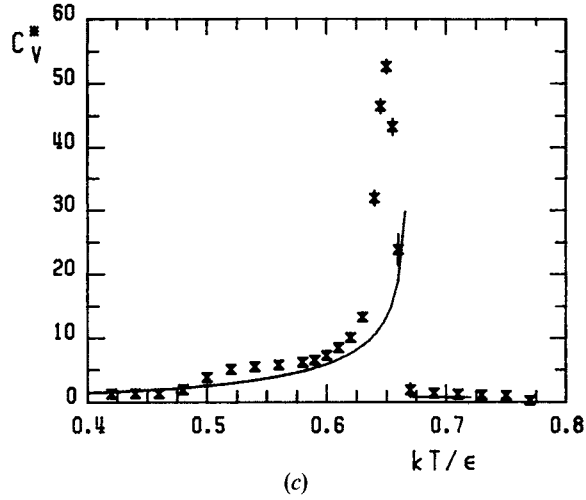

(*c*)

Figure 4. The temperature dependence of the heat capacity C_V^* for the P_4 model as obtained from PBMC on a $10 \times 10 \times 10$ lattice (*a*) CMC simulation on a $6 \times 6 \times 6$ lattice (*b*) and $10 \times 10 \times 10$ (*c*) compared with two site cluster results (continuous line).

The transition temperatures $(T^*_{NI})_{C_v}$ and $(T^*_{NI})_D$ obtained from the heat capacity and order parameter derivatives. The peak values C^*_{max} and $[d\langle P_2\rangle/dT^*]_{min}$ are also reported. The order parameters $\langle P_L\rangle_{NI}$ for the PBMC and CMC simulations are $\langle P_L\rangle_\lambda$ and $\langle P_L\rangle$ respectively as described in the text.

Method	$(T^*_{NI})_{C_v}$	C^*_{max}	$\langle P_2\rangle_{NI}$	$\langle P_4\rangle_{NI}$	$(T^*_{NI})_D$	$[d\langle P_2\rangle/dT^*]_{min}$
PBMC (10^3)	0·645 ± 0·05	30 ± 2	0·51 ± 0·07	0·58 ± 0·08	0·645 ± 0·05	−19·8 ± 0·09
CMC (6^3)	0·640 ± 0·08	39 ± 1	0·59 ± 0·07	0·64 ± 0·04	0·635 ± 0·05	−17·2 ± 0·6
CMC (10^3)	0·650 ± 0·05	53 ± 1	0·45 ± 0·08	0·54 ± 0·06	0·645 ± 0·05	−25·3 ± 0·6
MF	0·751	—	0·430	0·561	—	—
TSC	0·663	—	0·464	0·584	—	—

required for that. However, we notice that the first order character of the transition is enhanced in the P_4 model as compared to the more familiar P_2 (Lebwohl–Lasher model). This is consistently indicated by mean field and two site cluster theory as well as simulations on lattices of the same size (cf. [17] and references therein).

4.2. *Long range order parameters* $\langle P_2\rangle$, $\langle P_4\rangle$

We have calculated second and fourth rank order parameters $\langle P_2\rangle$, $\langle P_4\rangle$ for each simulation. The second rank order parameter $\langle P_2\rangle_\lambda$ obtained as the largest eigenvalue of the ordering matrix is shown as the open symbols in figures 5(*a*)–(*c*). As we know [7] this order parameter quantifies alignment with respect to the instantaneous director. We see an abrupt change of the order parameter at the transition for all the systems. In figure 5(*a*) we also show as the full squares the same quantity $\langle P_2\rangle_\lambda$ obtained from a separate simulation run in a cooling sequence starting from an isotropic phase. We see that very little hysteresis is observed and that the results of the two simulations are practically superimposable. This provides a check of the equilibration procedure and of the overall reliability of the calculations. One of the characteristics of the CMC method is the introduction of a director for the ghost particles and thus implicitly of a symmetry breaking direction which can be used to compute order parameters as

$$\langle P_L\rangle = \frac{1}{N}\left\langle \sum_i P_L(\cos\beta_i)\right\rangle. \tag{30}$$

These laboratory order parameters are shown in figures 5(*b*), (*c*) as the full symbols. We note the close agreement of the order parameters calculated in the two ways for the nematic phase. In the isotropic region the laboratory order parameter is essentially zero even for the small 6 × 6 × 6. We also plot in the same figures the mean field (dashed line) and the two site cluster predictions. We see that for this system the TSC method offers a good approximation to the temperature variation of $\langle P_2\rangle$. The abrupt change of order parameter, as well as the heat capacity peak seen earlier on are suggestive of a first order transition. Further insight is given by an examination of the spread of values of the order parameters at the different temperatures. In figure 6 we present histograms of the frequency of occurrence of $\langle P_2\rangle_\lambda$ and $\langle P_4\rangle_\lambda$ from the PBMC simulation. It seems quite clear, especially from the fourth rank order parameter, that the system does not gradually evolve from order to disorder

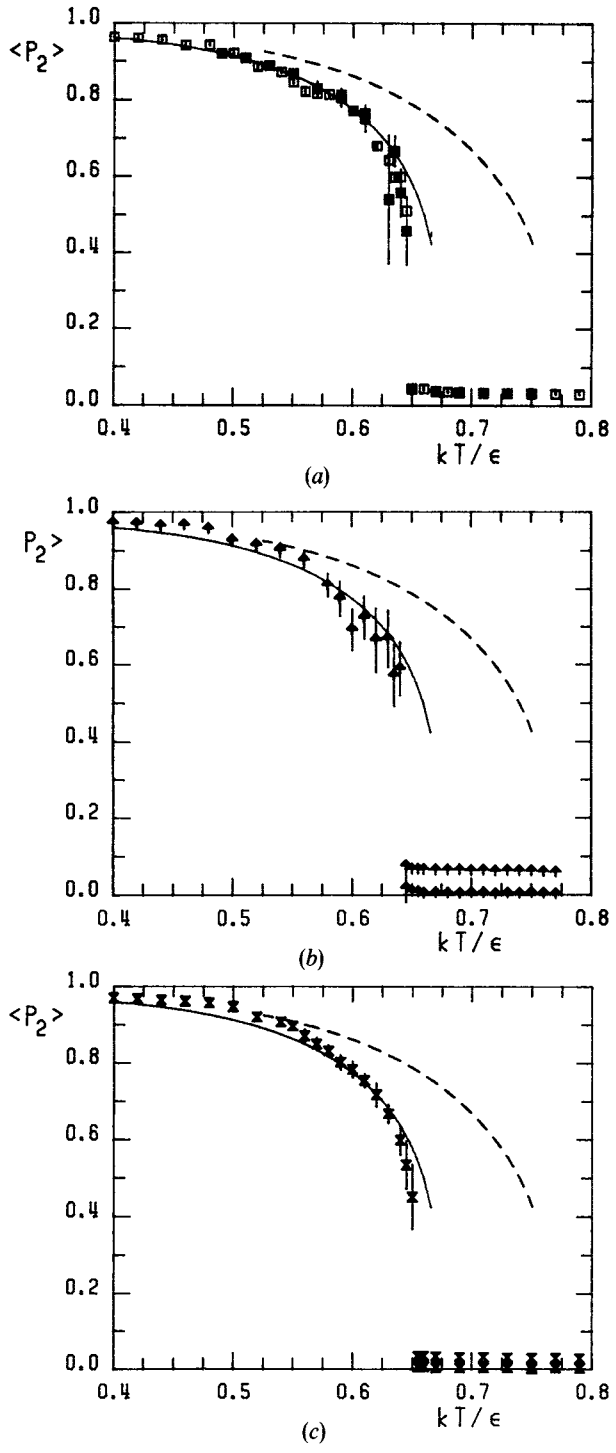

Figure 5. The second rank order parameters $\langle P_2 \rangle_\lambda$ obtained from a $10 \times 10 \times 10$ lattice PBMC (*a*), $6 \times 6 \times 6$ CMC (*b*) and $10 \times 10 \times 10$ lattice CMC (*c*), represented with open symbols. The full symbols give $\langle P_2 \rangle$ referred to the laboratory z axis for the two CMC simulations (*b*), (*c*) and instead $\langle P_2 \rangle_\lambda$ for a PBMC simulation started from isotropic (*a*). We also show the two site cluster (continuous line) and mean field theory curve (dashed lines).

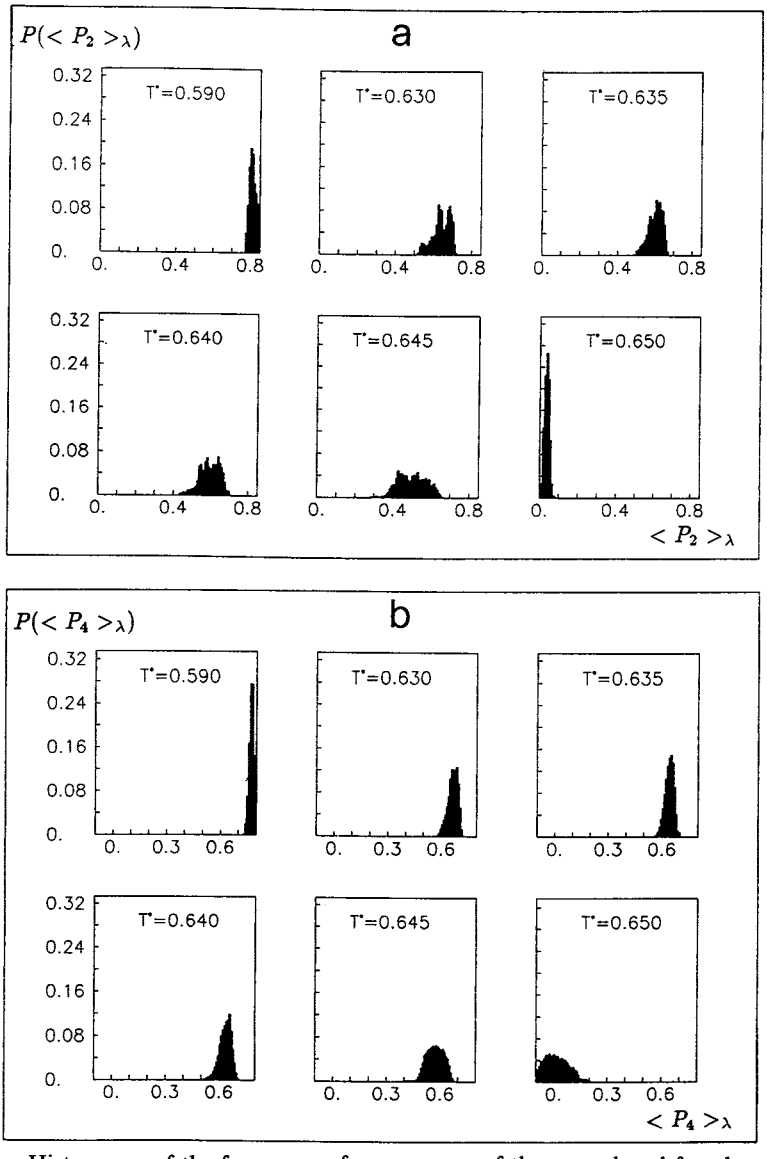

Figure 6. Histograms of the frequency of occurrences of the second and fourth rank order parameters $\langle P_2 \rangle_\lambda$ (*a*) and $\langle P_4 \rangle_\lambda$ (*b*) as obtained from PBMC on the $10 \times 10 \times 10$ lattice at the series of temperatures T^* indicated.

as the temperature increases. Rather the distribution of observed values is very well defined, with no long tail encompassing the nematic and isotropic value as observed in the Lebwohl–Lasher model [17]. The system jumps discontinuously, to our resolution, from a well ordered to a disordered state at a temperature between $T^* = 0{\cdot}645$ and $T^* = 0{\cdot}650$. The location of the phase transition is also confirmed by the peak in the derivative of the order parameter versus temperature given in the table. Our estimated values for the order parameters at the transition are reported in the table. The errors are quite large since the decay to zero is very steep.

It is interesting to plot $\langle P_4 \rangle$ against $\langle P_2 \rangle$ to see if the peculiar behaviour obtained in molecular field theory [1] is borne out by the simulations. In figure 7 we present the results for the three simulations together with the molecular field curve. There is good agreement in all cases, with the curve having the same characteristic shape and being quite different from, e.g., that of the Lebwohl–Lasher model [17]. The two site cluster results are shown in figure 8 as the circles and we see that once again they are confirming the results obtained from molecular field theory [1] reported as the continuous curve. In particular we see that in all cases there is a temperature region where $\langle P_4 \rangle$ is greater than $\langle P_2 \rangle$. The $\langle P_4 \rangle$ vs. $\langle P_2 \rangle$ curve obtained using TSC theory is essentially the same as that obtained from molecular field theory. Thus it seems worth while to try and find an analytic approximation to the curve, based on the known integral representation obtained from molecular field theory [24]. This theory [1] predicts the effective potential to be

$$-U(\cos\beta)/kT = a_4 P_4(\cos\beta). \tag{31}$$

We start by Taylor expanding the expressions for $\langle P_2 \rangle$ and $\langle P_4 \rangle$, i.e.

$$\langle P_L \rangle = \frac{\int_0^\pi d\beta \sin\beta P_L(\cos\beta) \exp\{a_4 P_4(\cos\beta)\}}{\int_0^\pi d\beta \sin\beta \exp\{a_4 P_4(\cos\beta)\}}, \qquad L = 2, 4, \tag{32}$$

with respect to a_4. This gives the first few terms as

$$\langle P_2 \rangle = \frac{10a_4^2}{693} + \frac{10a_4^3}{3003} + \frac{1010a_4^4}{26189163} - \frac{83990a_4^5}{909431523} - \frac{745490a_4^6}{70475037633} + \frac{2044355710a_4^7}{1626164510023053} + \ldots \tag{33}$$

and

$$\langle P_4 \rangle = \frac{a_4}{9} + \frac{9a_4^2}{1001} - \frac{1367a_4^3}{1378377} + \frac{457a_4^4}{2909907} + \frac{119776729a_4^5}{5426577897741} - \frac{48439a_4^6}{16326461151} + \frac{94079688551a_4^7}{106629930014368761} - \ldots \tag{34}$$

Reversion of the series for $\langle P_4 \rangle$ gives a_4 in terms of $\langle P_4 \rangle$, which substituted in equation (33) gives $\langle P_2 \rangle$ in terms of $\langle P_4 \rangle$ and by further reversion

$$\langle P_4 \rangle = \sqrt{\frac{77}{90}} \langle P_2 \rangle^{1/2} - \frac{69}{260} \langle P_2 \rangle + \frac{7794479}{1007760\sqrt{(770)}} \langle P_2 \rangle^{3/2} + \ldots. \tag{35}$$

This simple power series in $\sqrt{\langle P_2 \rangle}$ gives a good representation of the curve for $\langle P_2 \rangle$ up to 0.9. In figure 8 we show the analytical approximation to the $\langle P_4 \rangle$ vs. $\langle P_2 \rangle$ curve from the truncation in (35) (dashed line) and the curve obtained by direct numerical integration (continuous line).

4.3. *Pair properties*

We have calculated the second and fourth rank pair correlation coefficients $G_2(r)$ and $G_4(r)$,

$$G_L(r) = \langle P_L(\cos\beta_{ij}) \rangle_r \tag{36}$$

giving the orientational correlation between two particles i and j separated by a distance r. We have seen elsewhere that these represent the first two coefficients in the expansion of the rotationally invariant angular correlation function [7, 17]. The calculation of pair correlations is very time consuming and has only been performed at a few selected temperatures. As an illustration we show in figure 9 $G_2(r)$ as obtained from the CMC simulation of the $10 \times 10 \times 10$ system at a temperature below ($T^* = 0{\cdot}500$) and above ($T^* = 0{\cdot}790$) the transition. We have joined the points by the continuous line just as a guide to the eye. We see that the decrease of orientational correlation is quite regular. In the nematic the decay is to the usual

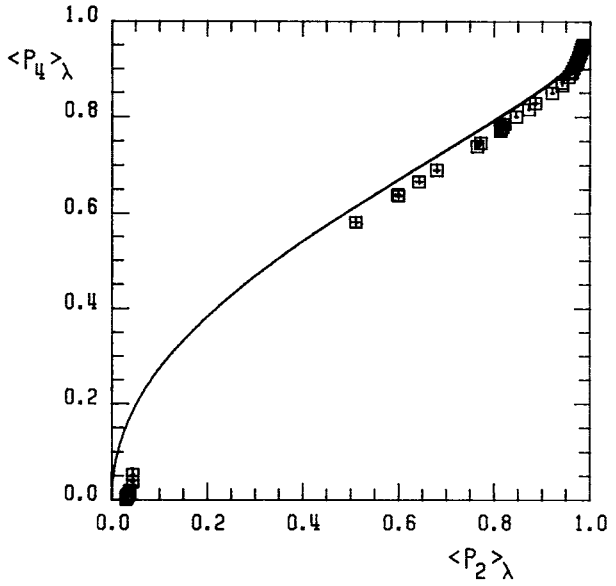

(*a*)

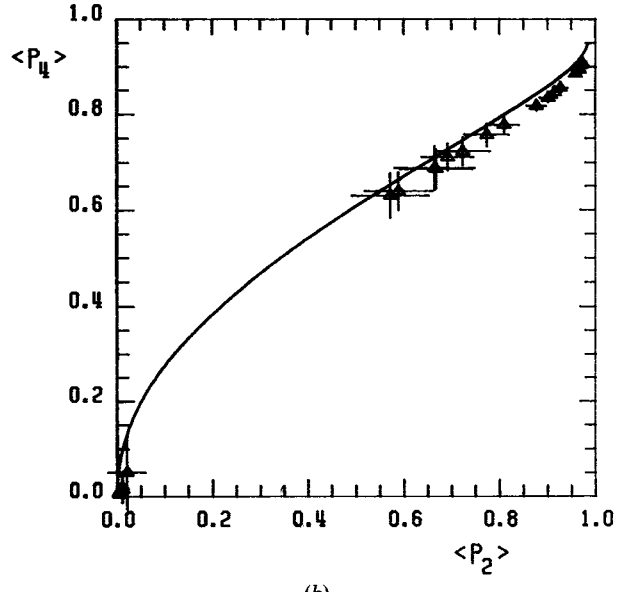

(*b*)

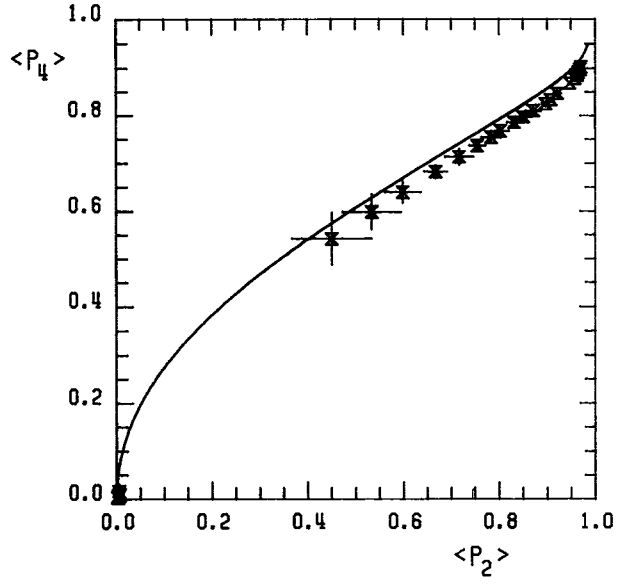

(*c*)

Figure 7. The fourth rank order parameter $\langle P_4 \rangle_\lambda$ as obtained from $10 \times 10 \times 10$ lattice PBMC (*a*) $6 \times 6 \times 6$ CMC (*b*), and $10 \times 10 \times 10$ lattice CMC (*c*) plotted against $\langle P_2 \rangle_\lambda$. We also show the molecular field (or two site cluster) curve (continuous line).

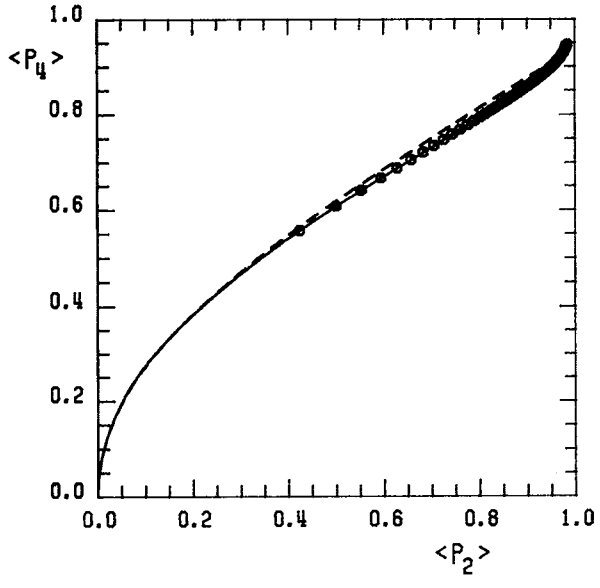

Figure 8. The fourth rank order parameter $\langle P_4 \rangle$ plotted vs. $\langle P_2 \rangle$. We show the molecular field curve as the continuous line and the two site cluster results as circles. We also show the analytical approximation in (35) (dashed line).

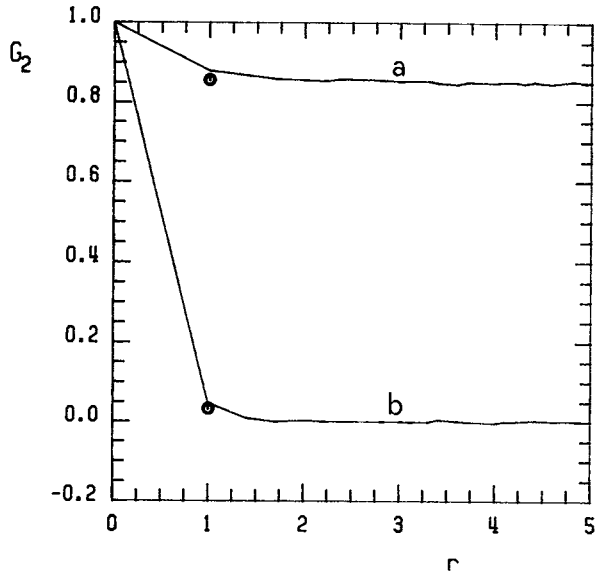

Figure 9. The second rank pair correlation coefficient plotted against separation r in lattice units as obtained from the CMC simulation with $N = 1000$ particles at $T^* = 0{\cdot}500$ (*a*) and $0{\cdot}790$ (*b*). A line is drawn through the points just to guide the eye. The symbols indicate the two site cluster result for the nearest neighbours value.

plateau $\langle P_2 \rangle^2$ [7]. In the isotropic phase the correlation quickly decays to zero. The two site cluster results for the nearest neighbours correlation, shown by the symbols, indicate a fair agreement. However, it is worth noticing that the decay of $G_2(r)$ is so fast that even at nearest neighbours distance we are already close to the long range limit indicated by the plateau.

A more interesting comparison is that in figure 10 where we present the tem-

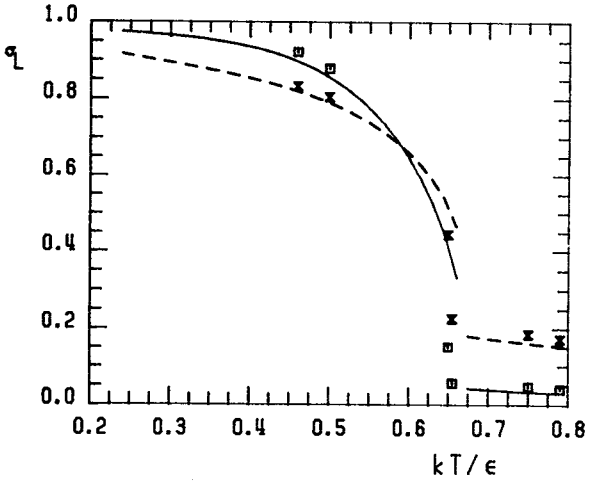

Figure 10. The second and fourth rank short range order parameters σ_2 (continuous line), σ_4 (dashed line) obtained from two site cluster theory plotted against reduced temperature. The symbols represent the $10 \times 10 \times 10$ CMC simulation results for σ_2 (square) and σ_4 (hour glass).

perature variation of the short range order parameters $\sigma_2 = G_2(a)$, $\sigma_4 = G_4(a)$ as obtained from two site cluster theory and from the CMC ($10 \times 10 \times 10$) simulation. We observe that TSC predicts the fourth rank nearest neighbours correlation to become larger than the second rank one at a high enough temperature. Moreover σ_4 is predicted to be bigger than σ_2 above the transition. Both these predictions are supported by the simulation and the agreement between the two sets of results is quite good.

5. Conclusions

The results of our simulations are consistent with a first order nematic–isotropic transition. The transition temperature is in good agreement with that predicted by two site cluster theory, while that obtained from molecular field theory is roughly 20 per cent too high. The results for the second and fourth rank order parameters confirm instead both the molecular field and two site cluster findings. Indeed the $\langle P_4 \rangle$ vs. $\langle P_2 \rangle$ curve obtained from simulation is similar for molecular field, two site cluster and Monte Carlo. It indicates a dominant P_4 character of the effective potential and broadly agrees with the experimental data of ref. [4–6]. The short range order parameter of fourth rank can also be greater than the second rank ones in a temperature region near the transition. This indicates a tendency of the particles to lie not only parallel but also perpendicular to one another both at short and long distance.

All calculations have been performed on a cluster of two DEC VAX 11-780 mini-computers at Dip. Fisica-INFN, Bologna and on a VAX 11-780 and VAX station at Dip. Chimica Fisica. C. Z. thanks C.N.R. and Min. P.I. for grants towards cost and maintenance of the latter systems.

References

[1] ZANNONI, C., 1979, *Molec. Crystals liq. Crystals Lett.*, **49**, 247.
[2] LEBWOHL, P. A., and LASHER, G., 1972, *Phys. Rev.* A, **6**, 426.
[3] ROSE, M. E., 1957, *Elementary Theory of Angular Momentum* (Wiley).
[4] AMELOOT, M., HENDRICKX, H., HERREMAN, W., POTTEL, H., VAN CAUWELAERT, F., and VAN DER MEER, W., 1984, *Biophys. J.*, **46**, 525.
[5] POTTEL, H., HERREMAN, W., VAN DER MEER, B. W., and AMELOOT, M., 1986, *Chem. Phys.*, **102**, 37.
[6] BEST, L., JOHN, E., and JÄHNIG, F., 1987, *Eur. J. Biophys.*, **15**, 87.
[7] ZANNONI, C., 1979, *The Molecular Physics of Liquid Crystals*, edited by G. R. Luckhurst and G. W. Gray (Academic Press), Chap. 9, p. 191.
[8] ZANNONI, C., 1986, *J. chem. Phys.*, **84**, 424.
[9] STRIEB, B., CALLEN, H. B., and HORWITZ, G., 1963, *Phys. Rev.*, **130**, 1798.
[10] SHENG, P., and WOJTOWICZ, P. J., 1976, *Phys. Rev.* A, **14**, 1883.
[11] YPMA, J. G. J., VERTOGEN, G., and KOSTER, H. T., 1976, *Molec. Crystals liq. Crystals*, **38**, 87.
[12] LEKKERKERKER, H. N. W., DEBRUYNE, J., VAN DER HAEGEN, R., and LUYCKX, R., 1978, *Physica* A, **94**, 465.
[13] LEVINE, R. D., and TRIBUS, M. (editors), 1979, *The Maximum Entropy Formalism* (MIT Press).
[14] 1982, *IMSL Library Reference Manual*, 9th edition (IMSL).
[15] NOMURA, S., KAMAI, H., KIMURA, I., and KAGIYAMA, M., 1970, *J. Polym. Sci.* A-2, **8**, 383.
[16] ABRAMOWITZ, M., and STEGUN, I. A. (editors), 1964, *Handbook of Mathematical Functions* (Dover).

[17] FABBRI, U., and ZANNONI, C., 1986, *Molec. Phys.*, **58,** 763.
[18] BARKER, J. A., and WATTS, R. O., 1969, *Chem. Phys. Lett.*, **3,** 144.
[19] CHATFIELD, C., 1983, *Statistics for Technology*, 3rd edition (Chapman & Hall).
[20] VAN DER HAEGEN, R., DEBRUYNE, J., LUYCKX, R., and LEKKERKERKER, H. N. W., 1980, *J. chem. Phys.*, **73,** 2469.
[21] JAMES, F., and ROOS, M., 1971, *MINUIT Minimization Package* (CERN Library), D506.
[22] CHICCOLI, C., PASINI, P., and ZANNONI, C., 1987, *Liq. Crystals*, **2,** 39.
[23] RUST, B., BURRUS, W. R., and SCHNEEBERGER, C., 1966 *Communs Ass. comput. Mach.*, **9,** 381.
[24] ZANNONI, C., 1988, *Polarized Spectroscopy of Ordered Systems*, edited by B. Samori' and E. Thulstrup (Kluwer), Chap. 3, p. 37.